Sensors & Actuators: B. Chemical 399 (2024) 134787

Contents lists available at ScienceDirect

Sensors and Actuators: B. Chemical

journal homepage: www.elsevier.com/locate/snb

Enzymeless electrochemical biosensor platform utilizing Cu_2O-Au nanohybrids for point-of-care creatinine testing in complex biological fluids

R.K. Rakesh Kumar [a,1], Amit Kumar [a,1], Muhammad Omar Shaikh [b], Chen-Yi Liao [c,*], Cheng-Hsin Chuang [a,d,**]

[a] Institute of Medical Science and Technology, National Sun Yat-Sen University, Kaohsiung 80424, Taiwan
[b] Sustainability Science and Management Program, Tunghai University, Taichung 407224, Taiwan
[c] Department of Internal Medicine, Kaohsiung Armed Forces General Hospital, Kaohsiung 802301, Taiwan
[d] Centre of Excellence for Metabolic Associated Fatty Liver Disease (CEMAFLD), National Sun Yat-Sen University, Kaohsiung 80424, Taiwan

ARTICLE INFO

Keywords:
Cu_2O-Au nanohybrid
POC creatinine testing
Enzyme-free biosensor
Zwitterion functionalization

ABSTRACT

Herein, we developed a novel, enzyme-free electrochemical biosensor that can directly quantify creatinine within complex biological fluids in a highly specific and sensitive manner. Our approach utilizes the synergistic effects of zwitterion-functionalized Cu_2O-Au core satellite nanohybrids with sophisticated 3D granular structures, which were synthesized via a rapid room-temperature combinatory protocol. Through nanoscale zwitterion surface engineering, outstanding antifouling capabilities were obtained and interferents were effectively eliminated by generating a pseudo proton exchange membrane (PEM). This pseudo-PEM can potentially serve as an alternative to traditional methods of removing interference; thus, analytes can be directly detected in untreated biofluids. The optimized biosensor platform demonstrated a linear response to creatinine with exceptional reproducibility and an excellent limit of detection (LOD) in the following sensing ranges: (i) 10.0–200 μM (R^2 =0.99, RSD=1.22 %, n = 10, LOD=0.72 μM) and (ii) 1.00–35.0 mM (R^2 =0.99, RSD=1.32 %, n = 10, LOD=2.41 mM). These ranges are clinically relevant and cover the entire physiological range of creatinine in human serum and urine, respectively. Furthermore, we successfully detected creatinine directly in untreated human urine samples and observed a high correlation with clinically determined values (r = 0.98). Overall, our proposed biosensor platform offers significant improvements over existing methods and provides a reliable and efficient approach for practical point-of-care (POC) creatinine quantification.

1. Introduction

Creatinine is an extensively studied biomolecule and the second most significant biomolecule in the clinic, with only glucose ranking higher. As a versatile biomarker, creatinine is used to perform diagnoses, monitor treatments, and provide prognoses for various muscular [1], cardiovascular [2], and renal diseases [3,4]. Creatinine is a byproduct of creatine metabolism and is typically excreted by the kidneys at a constant rate, regardless of hydration levels [5]. As a result, creatinine is an ideal internal standard molecule for calibrating other urinary biomarkers [6]. The levels of creatinine are precise markers for the early detection of acute muscle loss [7] and can also indicate renal damage caused by certain drugs [8] and surgical interventions [9]. Additionally, creatinine levels determine the glomerular filtration rate (eGFR) and the urinary albumin-to-creatinine ratio (ACR), which are clinical markers for kidney damage associated with renal dysfunctions, such as chronic kidney disease (CKD). CKD has a significant global burden, directly contributing to 1.2 million deaths, 19 million disability-adjusted life--years, and 18 million years of life lost. The disease is also closely linked to cardiovascular disorders [10]. Considering the high mortality rate of end-stage CKD and its asymptomatic nature in the early stages, early diagnosis is crucial to ensure timely and appropriate treatment, leading to improved survival rates [11]. Furthermore, the recent pandemic has underscored the impact of kidney disease on increased in-hospital mortality among patients with COVID-19 [12].

The current gold standard for creatinine quantification, which

* Corresponding author.
** Corresponding author at: Institute of Medical Science and Technology, National Sun Yat-Sen University, Kaohsiung 80424, Taiwan.
E-mail addresses: ericliao0217@gmail.com (C.-Y. Liao), chchuang@imst.nsysu.edu.tw (C.-H. Chuang).
[1] R. K. Rakesh Kumar and Amit Kumar have equally contributed to this work.

https://doi.org/10.1016/j.snb.2023.134787
Received 7 July 2023; Received in revised form 7 October 2023; Accepted 12 October 2023
Available online 20 October 2023

involves using the colorimetric Jaffé method, is susceptible to optical interferences and analytical inaccuracies, including temperature and variations in sample pH. Therefore, creatinine biosensing technologies that enable fast and reliable point-of-care analysis are being widely investigate [13]. Creatinine can be quantified in various biofluids, including saliva, sweat, tears, blood/serum, and urine; as a result, different detection techniques can be applied, such as colorimetric [14], spectroscopic [15], and chromatographic techniques [16]. However, sample handling in these traditional methods is complex and expensive, thus limiting their applicability in POC settings. Consequently, extensive research efforts have been focused on enabling creatinine analysis with reasonable clinical accuracy in a user-friendly manner [17]. Electrochemical biosensors have gained significant popularity for POC applications due to their sensitivity, reliability, cost-effectiveness, and simple detection mechanism, which allows for easy miniaturization and integration with portable readouts [18].

Various electrochemical methods for the quantification of creatinine have been reported in recent years, including those based on multienzyme-assisted decomposition of creatinine [19], electrochemical latent ratiometric probes [20], selective filtration through a functionalized membrane [21], antibody [22] or molecularly imprinted polymers (MIPs) [23] based affinity detection, and nanomaterial-assisted enzymeless detection [24]. Although highly specific, enzymatic biosensors are susceptible to external factors, such as pH and temperature [17]. Affinity-based biosensors offer robust stability but require cumbersome sample handling and long assay times. Conversely, selective membranes provide specificity but the sensitivity may be compromised due to changes in electrode surface morphologies. Alternatively, highly sensitive quantization based on the chelating ability of creatinine with transition metal ions, including Cu(II) in particular, has been successfully performed [25,26].

Previously, we demonstrated highly specific, enzyme-free electrochemical detection of creatinine in human serum utilizing zwitterion-functionalized Cu_2O nanoparticle (NP)-based biosensors [27]. The semiconductor nature of Cu_2O NPs limits the overall electron transfer capabilities of the sensing layer. Thus, the resulting in constrained sensing range restricts its application for creatinine detection in other biofluids, such as human urine. A realistic approach to improve the overall analytical performance is to increase the conductivity of Cu_2O nanocubes via nanohybridization with highly conductive metals, such as gold. Moreover, the synergistic effects of nanohybrids with complex nanostructures exhibiting novel properties and ambient stability have shown immense potential for enzyme-free biosensing technologies [28].

Herein, we report on the development of an enzyme-free electrochemical biosensor platform to accurately measure creatinine levels in human serum and urine utilizing zwitterion (N-hexadecyl-N,N-dimethyl-3-ammonio-1-propanesulfonate, hereon referred to as SB3C16)-functionalized Cu_2O-Au core satellite nanohybrids (SB3C16 @Cu_2O-Au), which exhibits four distinct nanostructures. As positive and negative charge centers are present, zwitterions are an ideal choice for antifouling. Sulfonate- and phenyl-based zwitterions are widely investigated as low-impedance coatings for enhanced specificity [29,30] The SB3C16 functionalization generates a proton exchange membrane (PEM), which provides excellent antifouling by electrostatically eliminating interferents. Under the established optimal conditions, the synergistic effects of the synthesized nanohybrid were utilized to develop a disposable, robust, and cost-effective enzyme-free electrochemical biosensor platform. The proposed biosensor demonstrated a fast response time, high specificity, and linear response to creatinine with outstanding reproducibility and excellent limit of detection (LOD) in the following sensing ranges: (i) 10.0–200 μM (R^2 =0.99, RSD=1.22 %, n = 10, LOD=0.72 μM) and (ii) 1.00–35.0 mM (R^2 =0.99, RSD=1.32 %, n = 10, LOD=2.41 mM). These sensing ranges are clinically relevant and cover the entire physiological range of creatinine in human serum and urine. To establish the feasibility of the developed biosensor for POC testing, we performed creatinine quantification directly in human urine samples. The accuracy of the biosensor was verified by comparing the results with clinically determined values, showing a high correlation (r = 0.98) and highlighting practical feasibility.

2. Methods/experimental

2.1. Materials

Copper (II) chloride dihydrate ($CuCl_2.2\ H_2O$, 99.99 %) was acquired from Alfa Aesar, N-hexadecyl-N,N-dimethyl-3-ammonio-1-propanesulfonate ($C_{24}H_{50}N_2O_4S$, ≥97.0 %), sodium L-ascorbate ($C_6H_7NaO_6$, ≥98 %), uric acid ($C_5H_4N_4O_3$, ≥99 %), potassium hexacyanoferrate(III) ($K_3Fe(CN)_6$, ≥ 99.0 %), potassium hexacyanoferrate(II) trihydrate ($K_4Fe(CN)_6.3\ H_2O$, 98.5–102.0 %), creatinine ($C_4H_7N_3O$, ≥98 %) human serum albumin (HSA powder, ≥99 %), actin (powder, ≥90 %), creatine ($C_4H_9N_3O_2$, ≥98 %), glucose ($C_6H_{12}O_6$, ≥99.5 %), ascorbic acid ($C_6H_8O_6$, ≥99 %), urea (NH_2CONH_2, ≥99.5 %), uric acid ($C_5H_4N_4O_3$, ≥99%), ammonia solution (NH_4OH, 25 %) and human serum (sterile-filtered) were purchased from Sigma Aldrich, phosphate-buffered saline (PBS) was purchased from UniRegion Bio-Tech, NaOH (pellets, 97 %) was purchased from SHOWA Chemical Co. Ltd. Artificial human urine was prepared using a previously reported protocol. All solutions were prepared in DI (ρ = 18.2 MΩ) unless mentioned otherwise.

2.2. Rapid room temperature synthesis of SB3C16-functionalized Cu_2O-Au core-satellite nanohybrid

An SB3C16-functionalized Cu_2O-Au core-satellite nanohybrid was synthesized at room temperature following two cardinal steps, which included a coreduction coupled rapid galvanic replacement reaction. The step-by-step schematics for the rapid room temperature synthesis of the SB3C16 @Cu_2O-Au core-satellite nanohybrid are given in Fig. 1(a). First, Cu_2O nanocubes were synthesized by adding 1.00 mL of NaOH (2.00 mM) to 40.0 mL of $CuCl_2$ (1.00 mM) followed immediately by 1.00 mL of sodium ascorbate (20.00 mM), which was then left undisturbed for 5 min. After the reaction was stirred for another 5 min with 0.20 g of SB3C1, the mixture was centrifuged at 8000 rpm for 15 min to generate SB3C16 @Cu_2O and was redispersed in DI water to generate solution 1 (2.50 mg/mL). Alternatively, four morphologically distinct SB3C16 @Cu_2O-Au core-satellite nanohybrids were prepared by adding (a) 0.50 mL, (b) 1.00 mL, (c) 2.00 mL, or (d) 3.00 mL of 1.50 mM $HAuCl_4$ dropwise to the reaction mixture containing unfunctionalized Cu_2O nanocubes under vigorous stirring for 15 min followed by 0.20 g of SB3C16 with an additional 5 min of stirring. The reaction mixture was then centrifuged at 8000 rpm for 15 min with DI water three times and redispersed in DI water to generate solution 2 (2.50 mg/mL).

2.3. Fabrication of SB3C16 @Cu_2O-Au core-satellite nanohybrid-modified electrodes

First, a screen-printed carbon electrode (SPCE) with a single working electrode design was fabricated using an inexpensive and scalable screen-printing process by printing nanomaterial-based carbon paste on a flexible PET substrate. The SPCE was then modified using a simple drop casting method, as shown in Fig. 1(b). Four different SPCEs were modified with SB3C16 @Cu_2O-Au core-satellite nanohybrid (referred to hereon as Electrode 1, Electrode 2, Electrode 3, and Electrode 4) by simply drop casting 10.0 μL, 15.0 μL, 20.0 μL and 25.0 μL of optimized solution 2, respectively, onto the surface of the working electrode and were set aside to dry under vacuum at 40 °C (Fig. 1b). This step eliminates moisture and facilitates binder-free adhesion of the SB3C16 @Cu_2O-Au core-satellite nanohybrid to the electrode surface. Additionally, a control electrode (referred to hereon as Electrode 5) was also fabricated using solution 1.

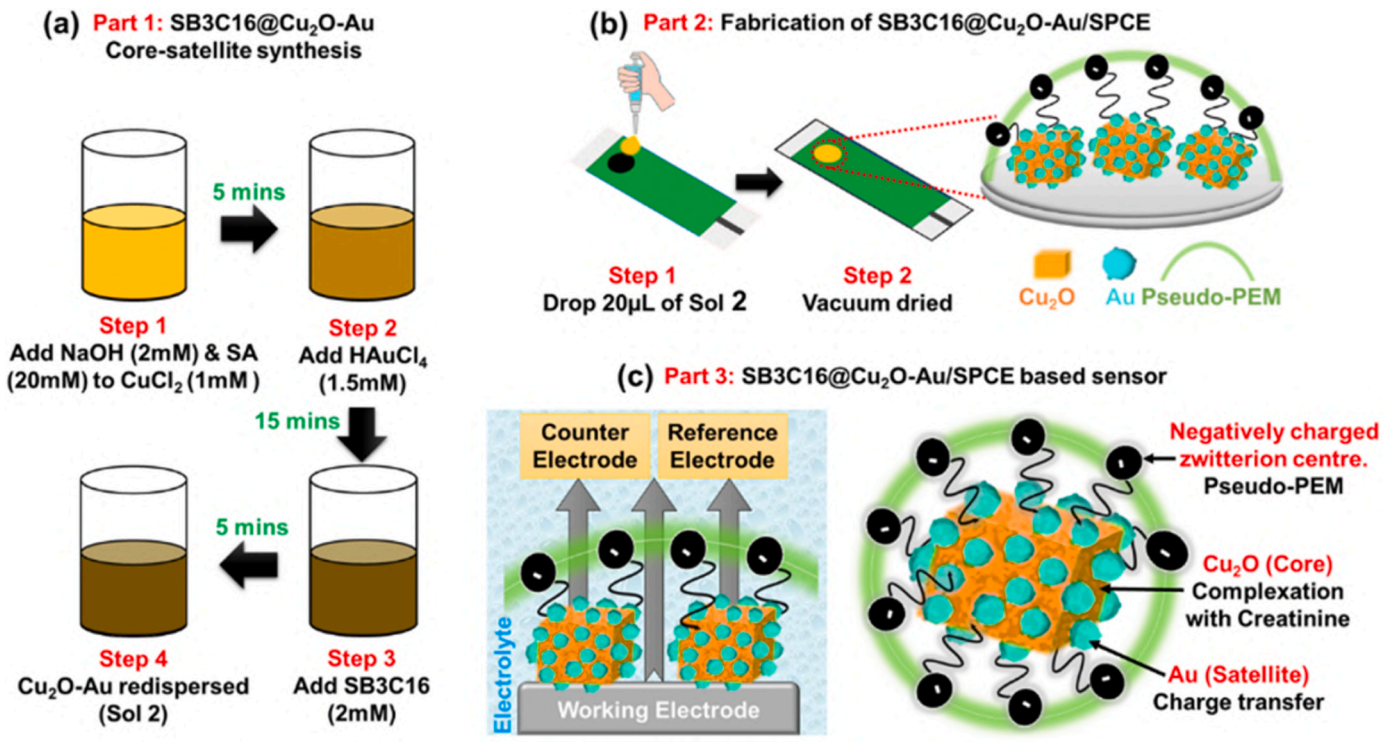

Fig. 1. Synthesis and fabrication. Step-by-step schematic representation of (a) rapid room temperature synthesis of SB3C16 @Cu_2O-Au core-satellite nanohybrid. (b) Fabrication of SB3C16 @Cu_2O-Au/SPCE-based modified electrode. (c) Schematic of the three-electrode electrochemical system used (left) and SB3C16 @Cu_2O-Au core-satellite nanohybrid (right).

2.4. Feasibility tests for POC creatinine quantification

The linear range and limit of detection (calculated as LOD=3.3 x standard deviation of the regression line (σ)/Slope) of the selected optimized electrodes for creatinine detection were investigated using differential pulse voltammetry (DPV) (potential range= 0.00–0.35 V, modulation= 0.25 scan rate= 100 mV/s) in 20.0 mM (PBS) solutions (maintained at pH=7.40 and pH=6.40 to mimic the pH conditions of real human serum and urine, respectively) spiked with creatinine concentrations varying between (i) 10.0 and 200 µM and (ii) 1.00 and 35.0 mM. Additionally, the observed background signal at zero creatinine concentration may induce inaccuracies. Thus, to ensure reliability, the biosensor response to creatinine was measured by normalizing the current variation observed during biosensing [$\triangle I = I$ (creatinine spiked) - I_o(Blank)] with the current value observed during blank scans [I_o(Blank)] as follows:

$$\text{Normalized current response}[\triangle I/Io]\% = \frac{\triangle I(\text{during biosensing})}{Io(\text{Blank})} \quad \text{x } 100.$$

The analytical concerns of the background signal were effectively eliminated by implementing this straightforward signal normalization. Finally, the normalized current response [$\triangle$I/Io]% to creatinine concentrations was translated to calibration graphs to determine the LOD for serum and urine-based creatinine quantification. Furthermore, the specificity of the SB3C16 @Cu_2O-Au core-satellite nanohybrid-based biosensor was investigated by performing two separate interference studies against interferents such as HSA, actin, creatine, glucose, ascorbic acid, urea, uric acid, and ammonia spiked in 20.0 mM PBS, which was maintained at pH= 7.40 and pH= 6.40 (the spiked concentrations are listed in Table S3). In addition, the stability of the modified electrodes was examined to demonstrate their robust shelf life by performing DPV scans in 20.0 mM PBS using modified electrodes stored under ambient conditions for extended time periods (180 days). Finally, the DPV signal response of the optimized electrodes to 10.0, 20.0, 40.0, 80.0 and 120 µM creatinine in fetal bovine serum (FBS) and 1.00, 5.00, 10.0, 15.0 and 20.0 mM creatinine in artificial urine was recorded to establish the accuracy and reliability of the developed biosensor.

2.5. Real sample analysis

Although clinical creatinine analysis is widely performed in serum, urine-based detection is better suited to realize biosensor-aided POC testing. Hence, the feasibility of the developed biosensor for direct creatinine quantification in untreated human urine was investigated. Primarily, ten urine samples (designated P1-P10) were collected from ten volunteers and stored at −80.0 °C prior to testing. Typically, each urine sample was introduced to the working surface of the developed biosensor at room temperature. The DVP signal response for each sample was collected, and the peak current, which was measured as the normalized current response [$\triangle$I/Io]%, was translated to its corresponding creatinine concentration. Additionally, the creatinine levels indicated by the developed biosensor were compared to the corresponding clinical results (obtained using a DXC 700 AU chemistry analyzer). Experiments involving human urine samples were performed according to protocols and guidelines approved by the Ethics Review Committee of National Sun Yat-sen University (Kaohsiung, Taiwan), and written consent was obtained from all participants.

3. Results/discussion

3.1. Characterization of the synthesized SB3C16@Cu_2O-Au core-satellite nanohybrid

A smooth template of Cu_2O nanocubes with a uniform size distribution (Fig. S1) was obtained by reducing $[Cu(OH)_4]^-$ with sodium ascorbate, as shown in Fig. 2(a). The subsequent addition of 1.5 mM $HAuCl_4$ solution induces island-mode growth of Au satellites at the surface of the Cu_2O core due to the simultaneous reduction of Au^{3+} in the presence of sodium ascorbate and the electroless galvanic replacement reaction (GRR) of Cu^{1+} with Au^{3+}, which favors a lower rate of

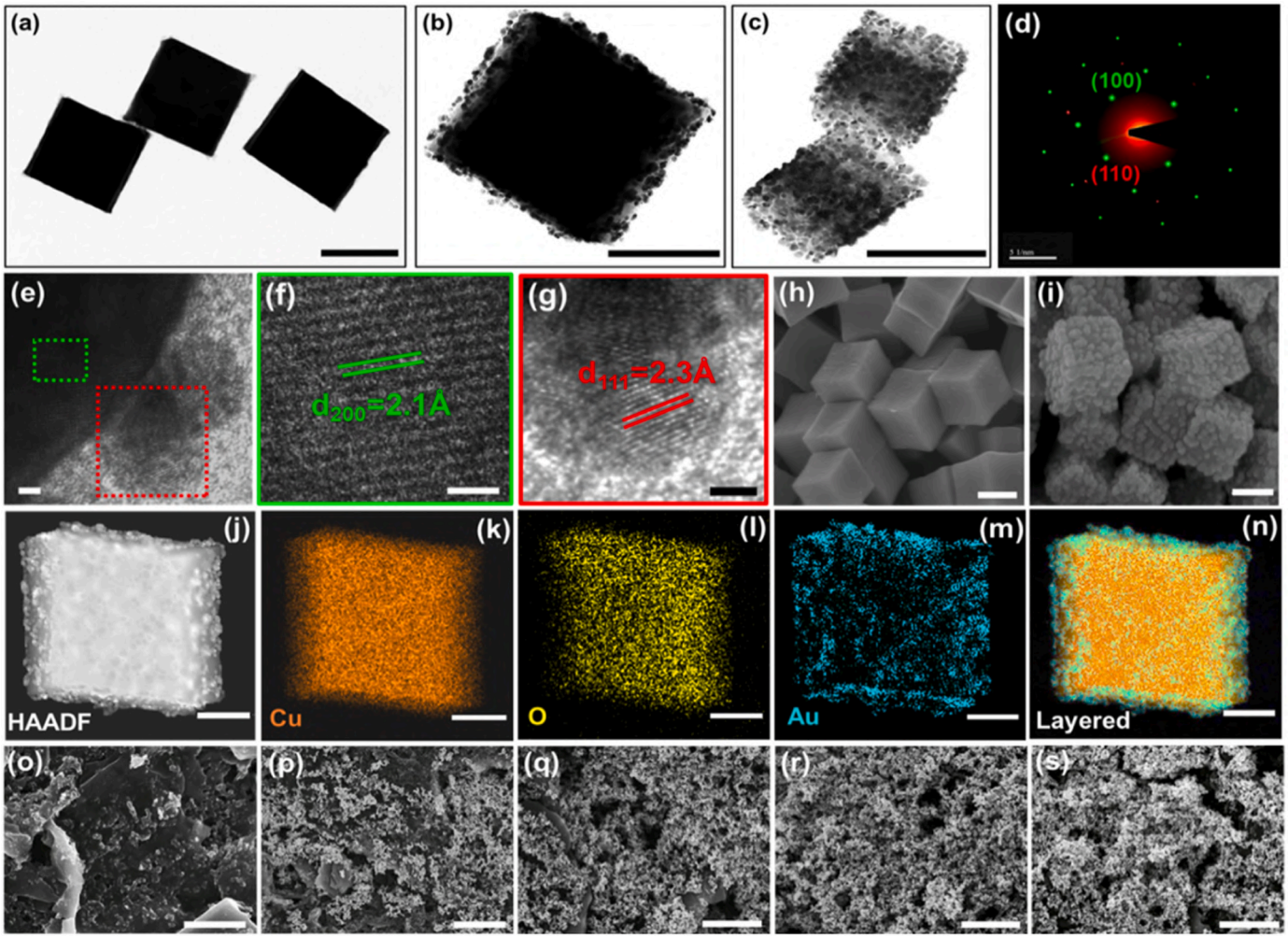

Fig. 2. Characterization of the SB31C6 @Cu_2O-Au core-satellite nanohybrid. High-resolution transmission electron micrographs of (a) SB31C6 @Cu_2O nanocubes and (b-c) SB31C6 @Cu_2O-Au core-satellite nanohybrid from two different viewing angles [Scale bar = 100 nm]. (d) SAED pattern of the synthesized SB31C6 @Cu_2O-Au core-satellite nanohybrid (green= Cu_2O, red=Au). (e) HRTEM image showing the lattice fringes in red and green that correspond to (f) the (200) plane of the Cu_2O core (green) and (g) the (111) plane of the Au satellite (red) with d spacings of 2.10 Å and 2.30 Å, respectively [Scale bar = 1 nm]. SEM micrographs of the (h) Cu_2O core and (i) SB31C6 @Cu_2O-Au core-satellite nanohybrid [Scale bar = 100 nm]. (j-n) Elemental analysis of the Cu_2O-Au core-satellite nanohybrid showing the elemental composition comprising Cu (orange), O (yellow) and Au (cyan) [Scale bar = 50 nm]. SEM images showing the surface morphologies of (o) bare SPCE and (p-s) modified electrodes (Electrodes 1, 2, 3 and 4). [Scale Bar= 1.00 μm].

surface diffusion at room temperature. Notably, Au^{3+} shows preferential absorption based on the surface energy of the template facets [31]. Hence, the utilization of the cubic template, which exhibits only (100) facets, ensures that the Au satellites grow uniformly on all surfaces of the cubical Cu_2O core. Thus, the extent of Au satellite deposition was effectively tailored by adjusting the volume of 1.5 mM $HAuCl_4$ solution added (0.50–2.00 mL) (Fig. S2 and Fig. S3). Cu_2O cores with uniformly deposited Au satellites (the calculated surface area coverage was 44.52 %), as shown in Fig. 2(b-c), were obtained at a $HAuCl_4$ volume of 1.50 mL and were therefore chosen as the optimal nanohybrid structure for further electrode modifications. The XRD patterns in Fig. S4 reveal the diffraction peaks of the Cu_2O core indexed solely to a single phase cubic cuprite crystal (JCPDS No. 65-3288) with a $Pn\bar{3}m$ space group and that of face centered cubic (FCC) Au nanoparticles (JCPDS No. 01-1172) [32,33]. The respective crystallographic planes with their peak positions (2θ) are listed in Table S1. Additionally, the layered SAED patterns in Fig. 2(d) and the lattice fringes in Fig. 2(e-g) with d spacings of 2.10 Å (green) and 2.30 Å (red) corresponding to the (200) and (111) planes of Cu_2O nanocubes and Au nanoparticles, respectively [34], validate that the synthesized Cu_2O core and Au satellites are single crystalline. SEM images contrasting the surface morphologies of the smooth Cu_2O nanocubes and the granular SB3C16 @Cu_2O-Au core-satellite nanohybrid are shown in Fig. 2(h-i).

Dense yet uniformly distributed Au satellites on the Cu_2O core were successfully observed using EDS elemental mapping analysis, as presented in Fig. 2(j-n). Furthermore, surface chemical characterization was performed using XPS, and the corresponding spectra are presented in Fig. S5. The XPS spectra at the core level show Cu $2p_{1/2,}$ Cu $2p_{3/2}$ and Cu LMM peaks at 952 eV, 932 eV and 570 eV, respectively, which were assigned exclusively to $Cu^{1+,}$ while the cuprite-associated oxygen peak in the O 1 s region was observed at 530 eV [35]. Finally, the peaks at 85.1 eV and 89.2 eV were attributed to Au $f_{5/2}$ and Au $f_{7/2}$ [28], respectively. Hence, the presence of a cuprite core with Cu in its + 1 oxidation state was validated, which was decorated with gold satellites with Au in its metallic state. Moreover, the presence of multiple Au satellites on the Cu_2O core triggers interband transitions and scattering, which can be seen as the broadening and blueshift of the UV—vis absorption peak of the Cu_2O core at 465 nm (Fig. S6) [36].

Fig. S7 shows the FTIR spectra of the unmodified Au-Cu_2O core-satellite nanohybrid depicting the characteristic peak of copper-oxygen stretching in the Cu_2O phase at 615 cm^{-1}. The additional IR signals for the SB3C16 @Au-Cu_2O core-satellite nanohybrid that

correspond to the C-N stretching signal at 1198 cm^{-1} and the S=O stretching peak at 1030 cm^{-1} confirm the presence of tertiary amine (since the broad N-H stretching peak at 3000–2800 cm^{-1} is absent) and sulfonate groups, respectively, which are the positive and negative centers of the SB3C16 zwitterion. The C-H bending signals at 755 cm^{-1}, 715 cm^{-1}, and 1465 cm^{-1} and C-H stretching signals were recorded at 2915 cm^{-1} and 2845 cm^{-1}. Moreover, zwitterion surface functionalization resulted in a significant negative shift in the zeta value from -14.8 ± 5 mV to -39.4 ± 4 mV, suggesting the preferential orientation of the negative head of SB3C16 ($-SO_3^-$) at the surface of the nanostructure (Fig. S8). The positive ($-N^+$) head of SB3C16 shows higher capabilities for interfacial orientation (relative to the negative head) [37], which integrally facilitates the colloidal stabilization of the developing Au-Cu_2O nanostructure. Thus, the negative head ($-SO_3^-$) faces outwards, resulting in a highly anionic surface environment that generates the pseudo proton exchange membrane (PEM).

3.2. Morphology of the nanohybrid-modified electrodes

The clear morphological differences of the flaky surface of the bare SPCE shown in Fig. 2(o) and the increasingly granular surface of electrodes 1–4, as shown in Fig. 2(p-s), verify that the SPCE was successfully modified using the simple drop-casting method. The granular morphology causes the nanohybrids to exhibit staggered positions, which inherently increases the electroactive surface area and leads to improved sensitivity compared to that of the smooth Cu_2O cores in Fig. 2 (h-i), which likely show hindered electron transfer due to surface-to-surface stacking. Notably, electrode 2 and electrode 3 in Fig. 2(q-r) exhibited ideal electrode surface morphologies with a homogeneous and uniformly thin layer of SB3C16 @Cu_2O-Au core-satellite nanohybrid. Although preliminary SEM micrographs indicate that electrode 2 and electrode 3 could exhibit superior electrochemical properties, further confirmatory investigations are needed to ascertain the optimal fabrication conditions, as discussed below.

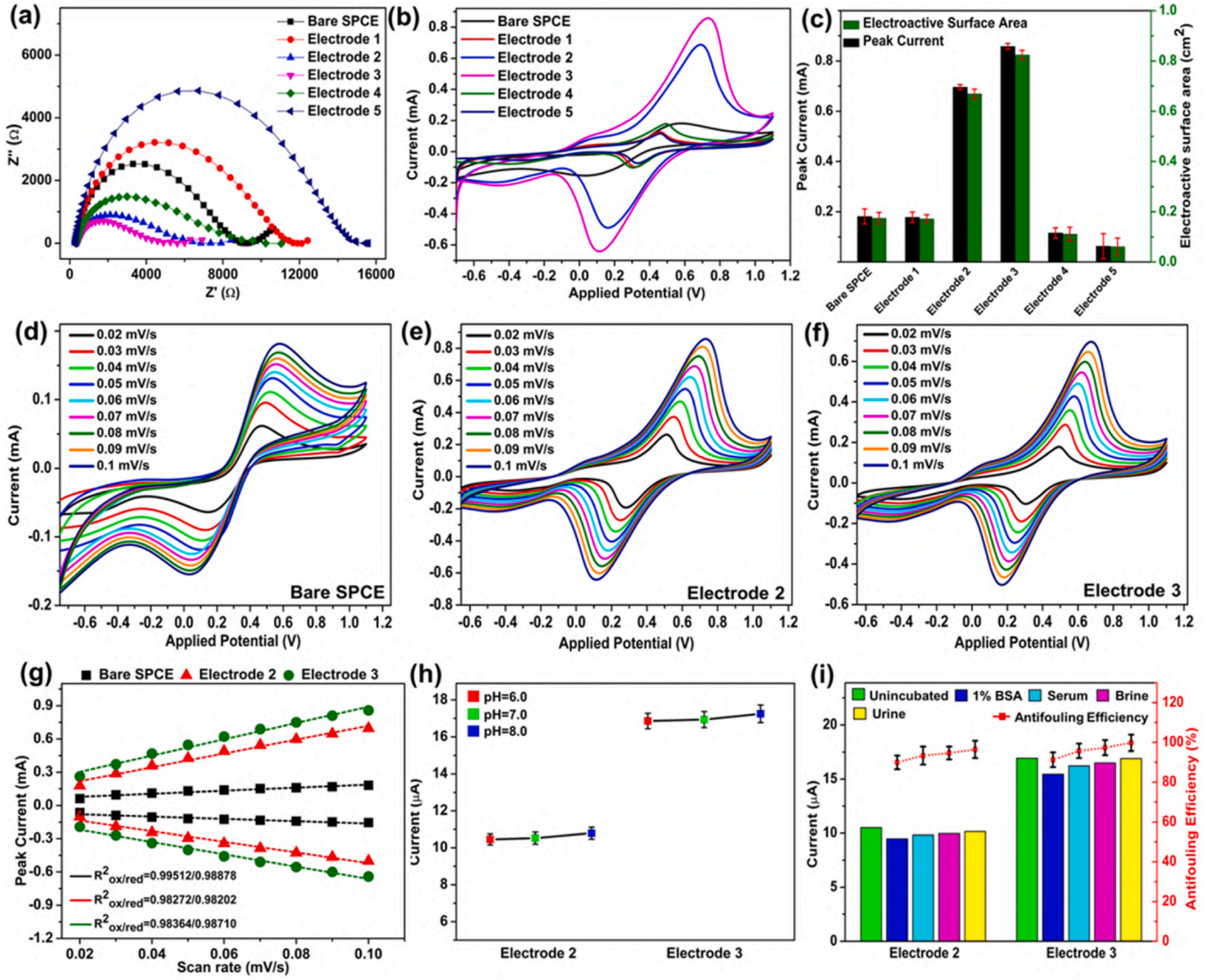

Fig. 3. Electrochemical characterization of SB31C6 @Cu_2O-Au core-satellite nanohybrid-modified electrodes. (a) Nyquist plots and (b) cyclic voltammograms (scan rate = 0.10 V/s) of bare SPCE, SB31C6 @Cu_2O-Au core-satellite nanohybrid-modified SPCE (Electrodes 1, 2, 3 and 4) and Cu_2O-modified SPCE (Electrode 5). (c) Comparative bar graph showing the peak current and the corresponding calculated electroactive surface area of the bare and modified electrodes. (d-f) Typical voltammograms showing oxidation and reduction peaks of bare SPCE, optimized electrode 2 and electrode 3 with varying scan rates (0.02 V/s- 0.10 V/s) in 5.00 mM $[Fe(CN)_6]^{2-}/[Fe(CN)_6]^{3-}$. (g) Oxidation/reduction peak current (ip) versus scan rate (v), extracted from the voltammograms shown in (d-f). (h) Electrochemical performance of the optimized electrodes under different pH conditions. (i) Antifouling capabilities of the fabricated optimized electrodes against 1 % BSA, human serum and brine and urine.

3.3. Electrochemical behavior of the modified electrodes

The modified electrodes exhibited diverse morphologies because the quantify of SB3C16 @Cu_2O-Au core-satellite nanohybrid present at the electrode surface varies, which predictably translates to distinct electrochemical behaviors. The electrochemical performance of the modified electrodes (namely, Electrodes 1–4) was investigated using electrochemical impedance spectroscopy (EIS). The corresponding Nyquist plots representing the semicircular impedance profiles of the bare and modified electrodes are shown in Fig. 3(a). The resistance to charge transfer (R_{ct}) was relatively small for electrodes 2 and 3, signifying superior charge transfer characteristics. Furthermore, the cyclic voltammograms in Fig. 3(b) depict high peak currents for electrodes 2 and 3. Finally, the observed peak current values were used to calculate the electroactive surface area of each electrode, as shown in Fig. 3(c). Under optimized fabrication conditions, the synergistic effect of the SB3C16 @Cu_2O-Au nanohybrid ensured ideal electrode performance, which is attributed to the catalytic nature of the Cu_2O core and the Au-mediated efficient charge transfer to the underlying SPCE. Additionally, due to the anchoring of the Au satellites, the SB3C16 @Cu_2O-Au nanohybrid possess an overall granular structure, thereby promoting a staggered position with adjacent nanohybrids. As a result, the electroactive surface area was effectively improved, enabling rapid electron transfer and ensuring excellent surface adhesion with the underlying SPCE. Conclusively, electrodes 2 and 3 exhibited high electroactive surface areas with superior charge transfer characteristics and were therefore determined to be the optimal modified electrodes. In addition, detailed simulations were conducted by constructing an equivalent circuit based on the Randles circuit, as shown in Fig. S9(a), which closely fit the observed impedance data, as shown in Fig. S9 (b-f) and Table S2. In addition, the transport behavior of charged species at the electrode-electrolyte interface of the bare SPCE and the optimized electrodes was also investigated using voltametric scan-rate studies. Fig. 3(d-f) shows typical sigmoidal voltammograms that revealed absorption-controlled diffusion profiles at low and high scan rates (0.02 V/s to 0.10 V/s). The peak oxidation/reduction currents were found to vary linearly with increasing scan rates (Fig. 3g), thereby indicating the presence of absorption-controlled electron transfer kinetics at the electrode-electrolyte interface. The optimized electrodes demonstrated excellent sensing stability, as evidenced by the minimal variations in the signal response to 10.0 μM and 1.00 mM creatinine in a pH range of 6.00–8.00 (Fig. 3h). Additionally, negligible differences in signal response were observed the optimized electrodes exhibited even after extended incubation in complex fluids, including 1 % bovine serum albumin (BSA), human serum, brine, and urine. This resilience toward variation in pH and sample fluid environments is attributed to the antifouling capabilities of the pseudo-PEM and indicates the possibility for directly detecting analytes without pH adjustment or sample purification steps.

3.4. Creatinine quantification in two distinct sensing ranges

Electrode 2 and electrode 3 were implemented as enzyme-free biosensors for electrochemical quantification of creatinine. The DPV curves of different concentrations of creatinine recorded using Electrode 2 and Electrode 3 are presented in Fig. 4(a) and (d), respectively. A directly proportional relationship between creatinine concentration and normalized peak current response [△I/Io]% with high reproducibility was observed in both cases. Electrode 2 exhibited an increasing DPV peak response with high linearity in the creatinine concentration range of 10.0–200 μM (R^2 =0.99, RSD=1.22 %, n = 10) covering the entire physiological range of creatinine in human serum (Fig. 4b). Similarly, electrode 3 demonstrated a linearly increasing DPV peak response in a creatinine concentration range of 1.00–35.0 mM (R^2 =0.99, RSD=1.32

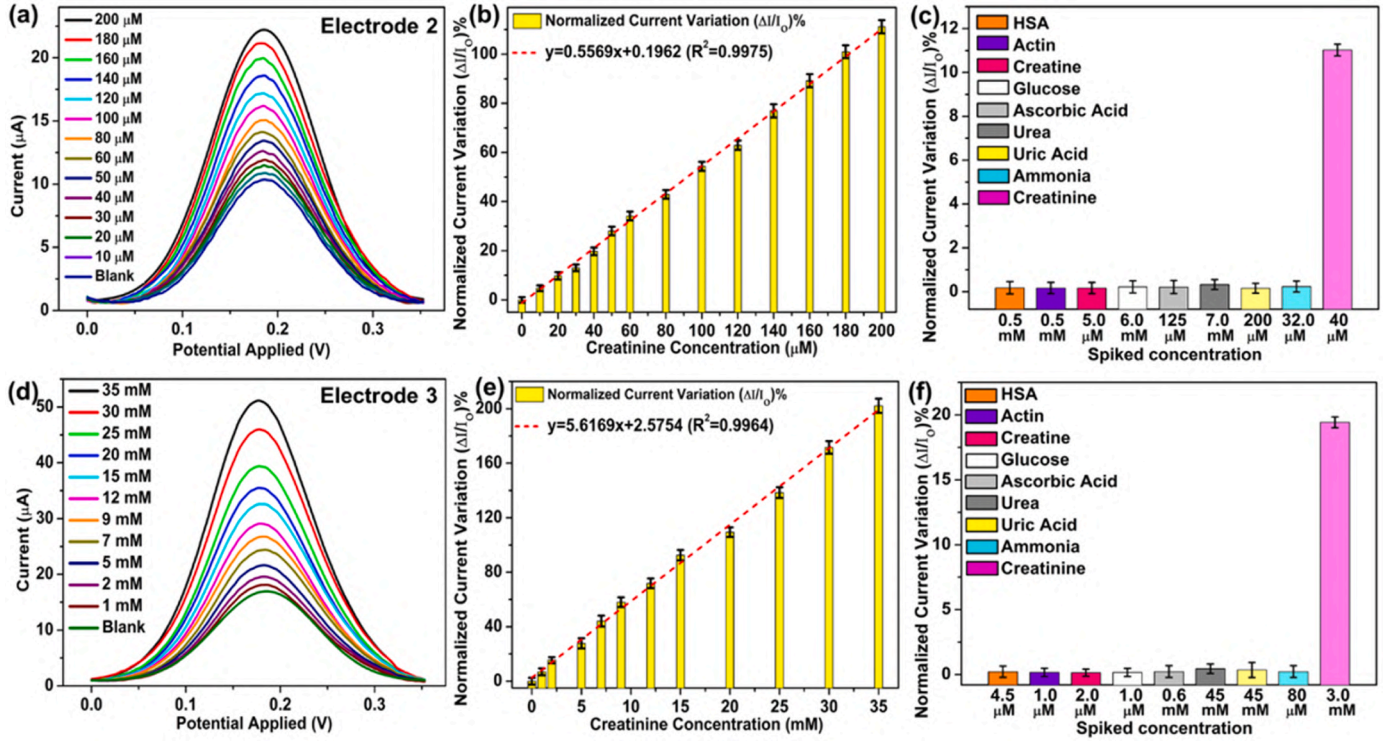

Fig. 4. Electrochemical quantification of creatinine. DPV response of optimized electrodes to varying creatinine concentrations ranging from (a) 10.0–200 μM (using electrode 2) and (d) 1.00–35.0 mM (using electrode 3), which covers the clinically relevant serum and urinary creatinine levels, respectively. Calibration curves displaying high linearity with small error bars demonstrating the feasibility and good reproducibility of the developed biosensor for creatinine quantification in (b) serum (R^2 =0.99, RSD=1.22 %, n = 10) and (e) urine (R^2 =0.99, RSD1.32 %, n = 10). Interference studies for (c) electrode 2 and (f) electrode 3 highlight the improved specificity observed owing to the presence of the zwitterion-enabled pseudo PEM.

%, n = 10), which encompasses both healthy and harmful creatinine levels in human urine (Fig. 4e). These two calibration curves can be represented by the linear equations (Serum) [△I/Io]%= 0.55 $C_{creatinine}$ (μM)+ 0.19, R^2 = 0.99 and (Urine) [△I/Io]%= 5.61 $C_{creatinine}$ (mM)+ 2.57, R^2 = 0.99. Accordingly, LODs of 0.72 μM and 2.41 mM (calculated as LOD= 3.3 x standard deviation of the regression line (σ)/slope) were observed for serum and urine creatinine quantification, respectively. The observed RSD values of 1.22 % and 1.32 % indicate excellent reproducibility, which results from the high homogeneity among the fabricated biosensors and emphasizing the potential for mass production. Moreover, storage stability is an important aspect in biosensor development that critically determines amenability to POC testing. Moreover, the design and fabrication of the optimized modified electrodes do not involve volatile components or organic enzymes; thus, the fabricated creatinine biosensors, namely, Electrodes 2 and 3, retained their original surface morphologies and electrochemical performance for sensitive creatinine detection even after a prolonged storage period of 180 days under ambient conditions (Fig. S10 and Fig. S11).

Finally, the specificity of the developed biosensor for creatinine was tested against physiological levels of major interferents, such as HSA, actin, creatine, glucose, ascorbic acid, urea, uric acid, and ammonia (Table S3). Fig. 4(c) and (f) shows the relatively marginal normalized current response for physiological levels of interferents (HSA, actin, creatine, glucose, ascorbic acid, urea, uric acid, and ammonia) against the superior response for 10.0 μM and 3.00 mM creatinine. These results highlight the outstanding specificity imparted by the zwitterion surface engineering of the Cu_2O-Au core-satellite nanohybrid, which generates a pseudo-PEM to electrostatically eliminate interferents. Additionally, creatinine quantification using the optimized electrodes in PBS maintained at pH values of 6.00, 7.00 and 8.00 resulted in overlapping DPV signal responses, as shown in Fig. S12. This result demonstrates the capability for creatinine detection in a wide pH range. In conclusion, the developed biosensor exhibited excellent specificity against major interferents and signal stability in a wide pH range. Therefore, biofluids, such as serum and urine, can be utilized to directly detect creatinine without pH adjustment or sample purification steps.

3.5. Sensing mechanism

The sensing mechanism was proposed based on the interpretations of three key observations. First, three consecutive DPV scans resulted in minimal variations in signal amplitude (<2.00 %), indicating a small electro-oxidative depletion of the nanohybrid layer [38]. However, as depicted in Fig. 5(a-b), the signal response to 200 μM and 35.0 mM

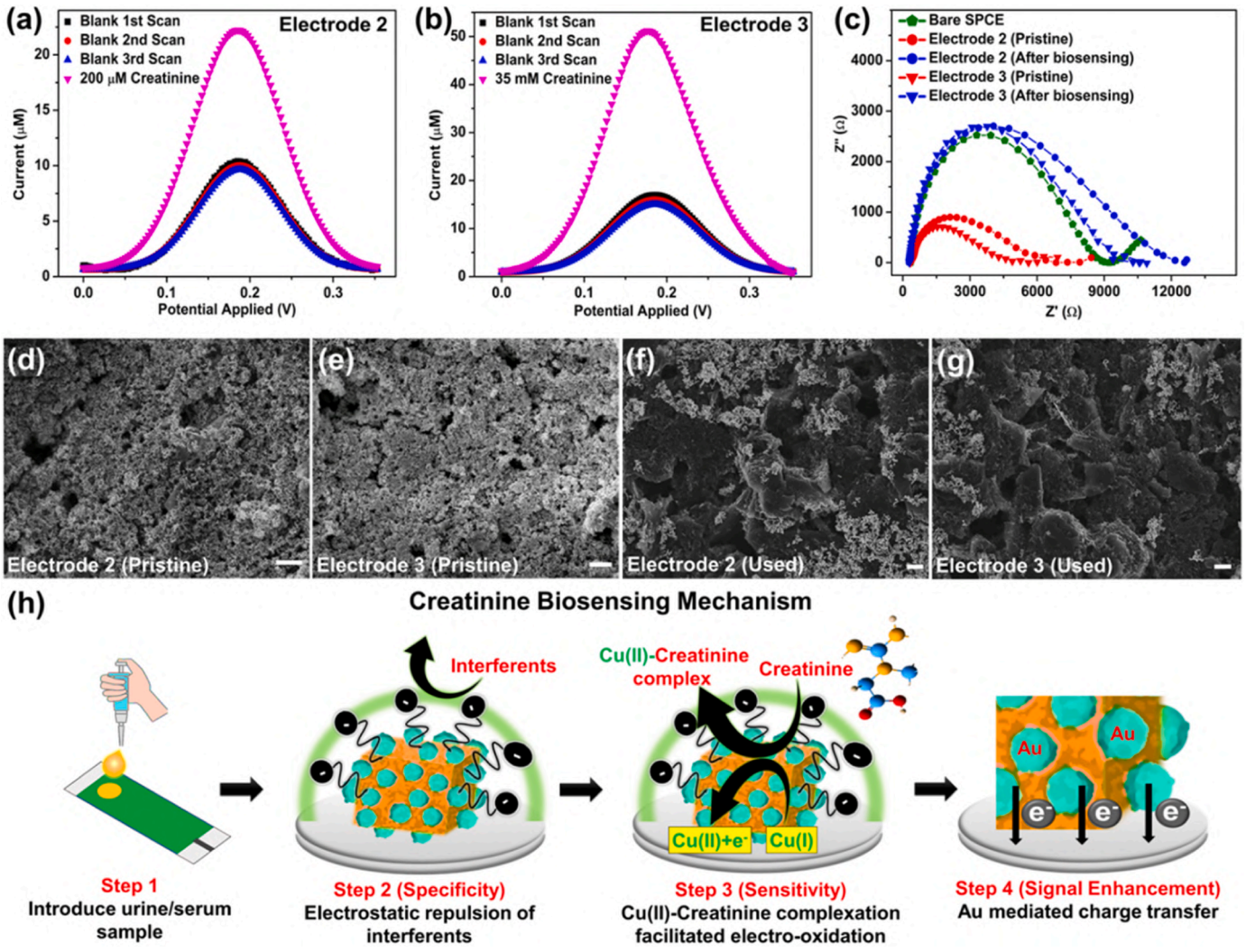

Fig. 5. Proposed creatinine sensing mechanism. DPV curves depicting the change in current response to three consecutive blank scans and in the presence of (a) 200 μM and (b) 35.0 mM creatinine. (c) Nyquist plots highlighting the change in R_{ct} of Electrode 2 and Electrode 3 after creatinine quantification. Scanning electron micrographs of pristine (d-e) and used (f-g) electrode 2 and electrode 3, respectively. (h) The proposed creatinine sensing mechanism, which involves adsorption-controlled Cu(II)-creatinine complexation coupled with a signal amplification step via Au-mediated charge transfer.

creatinine was significantly intensified by Electrode 2 and Electrode 3, respectively. This indicates the presence of a creatinine-dependent increase in the signal response. Second, EIS investigations of pristine and used biosensors in Fig. 5(c) indicated that the R_{ct} values increased due to depletion of the catalytic Cu_2O core and conductive Au satellites [39], as depicted by the SEM micrographs in Fig. 5(d-g). This depletion of the nanohybrid layer presumably results from electro-oxidation and dissolution of the Cu_2O core, which manifested as the observed variations in R_{ct}.

Based on the above observations, we propose a dual phase sensing mechanism in which each phase pertains to the specificity and sensitivity of the developed creatinine biosensor, as shown in Fig. 5(h). Herein, the specificity results from a negatively charged ionic shield (composed of the $-SO_3^-$ head of the SB3C16 zwitterion), which acts as a pseudo-PEM to electrostatically repel interferents from reaching the working electrode surface while facilitating the absorption of creatinine molecules; these molecules are known to exist as positively charged amino tautomers (pK_a= 4.89 at 20.0 °C) at physiological pH [5,40]. Concurrently, the sensitivity is directed by absorption-controlled soluble Cu(II)-creatinine complex formation initiated by potential-assisted electro-oxidation of Cu_2O from Cu(I) to Cu(II) accompanied by the generation of electrons. The Au satellites then facilitate the transfer of the generated electrons to the underlying SPCE, thus functioning as a signal amplifier. Primarily, the adsorbed creatinine at the electrode surface complexes with the free Cu^{2+} ions generated during the DVP scan (via delocalization of π electrons around the three endocyclic N atoms), thus forming a soluble Cu(II)-creatinine complex that goes into the test solution, thereby depleting the nanohybrid layer. The creatinine molecule thus acts as a scavenger for free Cu^{2+} at the electrode-electrolyte interface, thereby promoting the generation of more Cu^{2+}. Thus, electro-oxidation is improved, resulting in an amplified signal with increased creatinine concentrations.

3.6. Creatinine detection in spiked and real samples

The DPV signal response of electrode 2–10.0, 20.0, 40.0, 80.0 and 120 μM creatinine in fetal bovine serum (FBS) and that of electrode 3–1.00, 5.00, 10.0, 15.0 and 20.0 mM creatinine in artificial urine was recorded. The outstanding accuracy (%) presented in Fig. 6(a-b) indicates the excellent feasibility of the fabricated biosensor for highly sensitive and specific creatinine quantification in human serum and urine. Although clinical creatinine analysis is widely performed in serum, urine-based detection is better suited for the development of biosensors for POC testing. Hence, the viability of the developed biosensor (electrode 3) for direct creatinine quantification in untreated human urine was also investigated. The creatinine levels in urine samples collected from ten volunteers (designated P1-P10) were determined using the developed biosensor and were compared to the corresponding clinical results (obtained using a DXC 700 AU chemistry analyzer). The observed results and the calculated accuracy (%) of the biosensor are shown in Table S4. As depicted in Fig. 6(c), the creatinine concentrations established using the biosensor (Electrode 3) were found to possess a high correlation with the clinically quantified results (Pearson's r = 0.98). A comparative table highlighting the significant

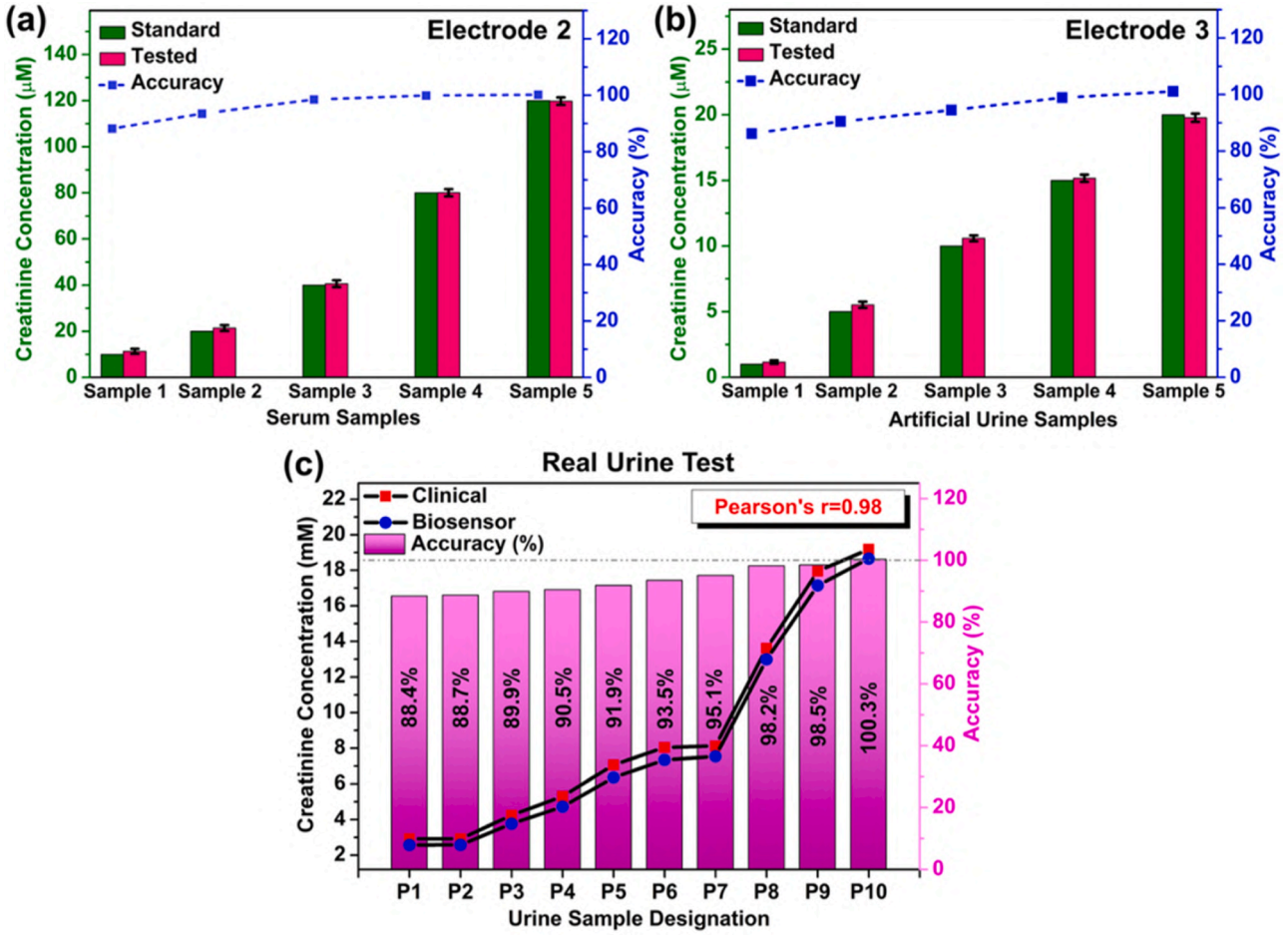

Fig. 6. Practical feasibility evaluation. Creatinine quantification in (a) spiked human serum with electrode 2 (n = 3) and (b) spiked artificial urine with electrode 3 (n = 3). (c) Determination of creatinine levels in real human urine collected from ten volunteers and correlation with the corresponding clinically determined values, demonstrating improved accuracy and a high Pearson's correlation coefficient (r = 0.98).

improvements of the developed biosensors over existing methods is also provided in Table S5.

4. Conclusion

In summary, we have developed a novel universal enzyme-free electrochemical creatinine biosensor platform that can directly quantify creatinine in untreated human urine utilizing the synergetic effects of zwitterion-functionalized Cu_2O-Au core satellite nanohybrids. In addition to a robust shelf life, the biosensor also established outstanding specificity and accuracy with reasonable inertness to variation in sensing conditions (such as pH); as a result, the presampling steps and stringent sensing parameters were eliminated, facilitating user-friendly sample handling and emphasizes the immense amenability of the developed biosensor for POC creatinine testing. The sensing mechanism primarily follows a potential assisted electro-oxidation of the Cu_2O core (Cu^{1+} to Cu^{2+}) and the consequent chelation of creatinine with Cu^{2+} to form a soluble Cu(II)-creatinine complex. Additionally, the highly conductive Au satellites facilitate the transfer of electrons generated during electro-oxidation for amplified signal generation. The pseudo PEM generated via nanoscale zwitterion surface engineering electrostatically eliminated interferents to ensure excellent specificity against major interferents (HSA, actin, creatine, glucose, ascorbic acid, urea, uric acid, and ammonia) and a minimal decrease in signal (<2.00 %) over an elongated storage period of 180 days. Moreover, the proposed zwitterion pseudo-PEM can be extended to other applications as a simple yet effective alternative to traditional cover layers, ensuring high specificity without compromising the surface morphology of the modified electrode.

CRediT authorship contribution statement

R. K. Rakesh Kumar, Amit Kumar have equally contributed to the work. **R. K. Rakesh Kumar** and **Amit Kumar** designed and conducted the experiments, analysed the results, and wrote the manuscript. **Muhammad Omar Shaikh** validated the experimental data. **Cheng-Hsin Chuang** and **Chen-Yi Liao** served as equally contributing corresponding authors who supervised and administrated the work.

Declaration of Competing Interest

The authors declare the following financial interests/personal relationships which may be considered as potential competing interests Cheng-Hsin Chuang reports financial support was provided by National Science and Technology Council. Cheng-Hsin Chuang has patent Method for generating charged pseudo exchange membrane pending to National Sun Yat-sen University.

Data availability

Data will be made available on request.

Acknowledgements

The authors would like to thank the Ministry of Science and Technology, Taiwan, for financially supporting this research under Contract No. MOST 107-2221-E-218 -030 -MY3.

Appendix A. Supporting information

Supplementary data associated with this article can be found in the online version at doi:10.1016/j.snb.2023.134787.

References

[1] K. Kashani, M.H. Rosner, M. Ostermann, Creatinine: from physiology to clinical application, Eur. J. Intern. Med. (2020) 9–14.
[2] M. Kanbay, L.A. Ertuglu, B. Afsar, E. Ozdogan, Z.S. Kucuksumer, A. Ortiz, A. Covic, M. Kuwabara, D.Z.I. Cherney, D.H. van Raalte, D. de Zeeuw, Renal hyperfiltration defined by high estimated glomerular filtration rate: a risk factor for cardiovascular disease and mortality, Diabetes Obes. Metab. (2019) 2368–2383.
[3] A. Kumar, R.K. Rakesh Kumar, M.O. Shaikh, C.H. Lu, J.Y. Yang, H.L. Chang, C. H. Chuang, Ultrasensitive strain sensor utilizing a AgF-AgNW hybrid nanocomposite for breath monitoring and pulmonary function analysis, ACS Appl. Mater. Interfaces (2022) 55402–55413.
[4] A.G. Bostom, F. Kronenberg, E. Ritz, Predictive performance of renal function equations for patients with chronic kidney disease and normal serum creatinine levels, J. Am. Soc. Nephrol. (2002) 2140–2144.
[5] R.K. Rakesh Kumar, M.O. Shaikh, C.H. Chuang, A review of recent advances in non-enzymatic electrochemical creatinine biosensing, Anal. Chim. Acta (2021), 338748.
[6] C.M. Bulka, S.L. Mabila, J.P. Lash, M.E. Turyk, M. Argos, Arsenic and obesity: a comparison of urine dilution adjustment methods, Environ. Health Perspect. (2017), 087020.
[7] K.K. Harmon, J.R. Stout, D.H. Fukuda, P.S. Pabian, E.S. Rawson, M.S. Stock, The application of creatine supplementation in medical rehabilitation, Nutrients (2021) 1825.
[8] S. Wiebe, D. Schnell, R. Külzer, D. Gansser, A. Weber, G. Wallenstein, A. Halabi, A. Conrad, S. Wind, Influence of renal impairment on the pharmacokinetics of afatinib: an open-label, single-dose study, Eur. J. Drug Metab. Pharmacokinet. (2017) 461–469.
[9] P. Priyanka, A. Zarbock, J. Izawa, T.G. Gleason, R.W. Renfurm, J.A. Kellum, The impact of acute kidney injury by serum creatinine or urine output criteria on major adverse kidney events in cardiac surgery patients, J. Thorac. Cardiovasc. Surg. (2021) 143–150.
[10] P. Cockwell, L.A. Fisher, The global burden of chronic kidney disease, Lancet (2020) 662–664.
[11] D.S. Tuot, L.E. Boulware, Telehealth applications to enhance CKD knowledge and awareness among patients and providers, Adv. Chronic Kidney Dis. (2017) 39–45.
[12] Y. Cheng, R. Luo, K. Wang, M. Zhang, Z. Wang, L. Dong, J. Li, Y. Yao, S. Ge, G. Xu, Kidney disease is associated with in-hospital death of patients with COVID-19, Kidney Int (2020) 829–838.
[13] T. Küme, B. Sağlam, C. Ergon, A.R. Sisman, Evaluation and comparison of Abbott Jaffe and enzymatic creatinine methods: could the old method meet the new requirements? J. Clin. Lab. Anal. (2018), e22168.
[14] J.R. Delanghe, M.M. Speeckaert, Creatinine determination according to Jaffe - What does it stand for? NDT (2011) 83–86.
[15] J.W. McMurdy, A.J. Berger, Raman spectroscopy-based creatinine measurement in urine samples from a multipatient population, Appl. Spectrosc. (5) (2003) 522.
[16] A. Mathaweesansurn, S. Thongrod, P. Khongkaew, C.M. Phechkrajang, P. Wilairat, N. Choengchan, Simple and fast fabrication of microfluidic paper-based analytical device by contact stamping for multiple-point standard addition assay: application to direct analysis of urinary creatinine, Talanta (2020), 120675.
[17] R. Cánovas, M. Cuartero, G.A. Crespo, Modern creatinine (Bio)sensing: challenges of point-of-care platforms, Biosens. Bioelectron. (2019) 110–124.
[18] A. Singh, A. Sharma, A. Ahmed, A.K. Sundramoorthy, H. Furukawa, S. Arya, A. Khosla, Recent advances in electrochemical biosensors: Applications, challenges, and future scope, Biosensors (2021) 336.
[19] EI. Tzianni, I. Moutsios, D. Moschovas, A. Avgeropoulos, K. Govaris, L. Panagiotidis, M.I. Prodromidis, Smartphone paired SIM card-type integrated creatinine biosensor, Biosens. Bioelectron. (2022), 114204.
[20] S. Kumaravel, S.H. Wu, G.Z. Chen, S.T. Huang, C.M. Lin, Y.C. Lee, C.H. Chen, Development of ratiometric electrochemical molecular switches to assay endogenous formaldehyde in live cells, whole blood and creatinine in saliva, Biosens. Bioelectron. (2021), 112720.
[21] Y. Liu, R. Cánovas, G.A. Crespo, M. Cuartero, Thin-layer potentiometry for creatinine detection in undiluted human urine using ion-exchange membranes as barriers for charged interferences, Anal. Chem. (2020) 3315–3323.
[22] A. Benkert, F. Scheller, W. Schössler, C. Hentschel, B. Micheel, O. Behrsing, G. Scharte, W. Stöcklein, A. Warsinke, Development of a creatinine ELISA and an amperometric antibody-based creatinine sensor with a detection limit in the nanomolar range, Anal. Chem. (2000) 916–921.
[23] Y. Li, L. Luo, M. Nie, A. Davenport, Y. Li, B. Li, K.L. Choy, A graphene nanoplatelet-polydopamine molecularly imprinted biosensor for Ultratrace creatinine detection, Biosens. Bioelectron. (2022), 114638.
[24] S.K. Ponnaiah, P. Prakash, Carbon dots doped tungstic anhydride on graphene oxide nanopanels: A new picomolar-range creatinine selective enzymeless electrochemical sensor, Mater. Sci. Eng. C (2020), 111010.
[25] J. Raveendran, P.E. Resmi, T. Ramachandran, B.G. Nair, T.G. Satheesh Babu, Fabrication of a disposable non-enzymatic electrochemical creatinine sensor, Sens. Actuators B Chem. (2017) 589–595.
[26] I. Pandey, P.K. Bairagi, N. Verma, Electrochemically grown polymethylene blue nanofilm on copper-carbon nanofiber nanocomposite: an electrochemical sensor for creatinine, Sens. Actuators B Chem. (2018) 562–570.
[27] R.K. Rakesh Kumar, M.O. Shaikh, A. Kumar, C.H. Liu, C.H. Chuang, Zwitterion-functionalized cuprous oxide nanoparticles for highly specific and enzymeless electrochemical creatinine biosensing in human serum, ACS Appl. Nano Mater. (2023) 2083–2094.

[28] R.K.R. Kumar, A. Kumar, C.H. Chuang, M.O. Shaikh, Electrochemical immunosensor utilizing a multifunctional 3D nanocomposite coating with antifouling capability for urinary bladder cancer diagnosis, Sens. Actuators B Chem. (2023), 133621.
[29] W.F. Chan, E. Marand, S.M. Martin, Novel zwitterion functionalized carbon nanotube nanocomposite membranes for improved RO performance and surface anti-biofouling resistance, J. Memb. Sci. (2016) 125–137.
[30] A.L. Gui, E. Luais, J.R. Peterson, J.J. Gooding, Zwitterionic phenyl layers: finally, stable, anti-biofouling coatings that do not passivate electrodes, ACS Appl. Mater. Interfaces (2013) 4827–4835.
[31] H.J. Jang, S. Ham, J.A.I. Acapulco, Y. Song, S. Hong, K.L. Shuford, S. Park, Fabrication of 2D Au nanorings with Pt framework, J. Am. Chem. Soc. (2014) 17674–17680.
[32] H. Azimi, S. Kuhri, A. Osvet, G. Matt, L.S. Khanzada, M. Lemmer, N.A. Luechinger, M.I. Larsson, E. Zeira, D.M. Guldi, C.J. Brabec, Effective ligand passivation of Cu2O nanoparticles through solid-state treatment with mercaptopropionic acid, J. Am. Chem. Soc. (2014) 7233–7236.
[33] T.K. Aparna, R. Sivasubramanian, M.A. Dar, One-pot synthesis of Au-Cu2O/rGO nanocomposite based electrochemical sensor for selective and simultaneous detection of dopamine and uric acid, J. Alloy. Compd. (2018) 1130–1141.
[34] W.H. Ke, C.F. Hsia, Y.J. Chen, M.H. Huang, Synthesis of ultrasmall Cu2O nanocubes and octahedra with tunable sizes for facet-dependent optical property examination, Small (2016) 3530–3534.
[35] C. Liu, M. Wang, J. Ye, L. Liu, L. Li, Y. Li, X. Huang, Highly Selective CO_2 electroreduction to C2+ products over Cu2O-Decorated 2D metal-organic frameworks with rich heterogeneous interfaces, Nano Lett. (2023) 1474–1480.
[36] S. Zhu, D. Deng, M.T. Nguyen, Y.T.R. Chau, C.Y. Wen, T. Yonezawa, Synthesis of Au@Cu2O core-shell nanoparticles with tunable shell thickness and their degradation mechanism in aqueous solutions, Langmuir (2020) 3380–3392.
[37] J.P. Priebe, F.D. Souza, M. Silva, D.W. Tondo, J.M. Priebe, G.A. Micke, A.C. O. Costa, C.A. Bunton, F.H. Quina, H.D. Fiedler, F. Nome, The chameleon-like nature of zwitterionic micelles: effect of cation binding, Langmuir (2012) 1758–1764.
[38] P.K. Kalambate, Z. Dhanjai, Y. Huang, Y. Li, M. Shen, Y. Xie, A.K. Huang, Srivastava, Core@shell nanomaterials based sensing devices: a review, TrAC Trends Anal. Chem. (2019) 147–161.
[39] O. Pänke, T. Balkenhohl, J. Kafka, D. Schäfer, F. Lisdat, Impedance spectroscopy and biosensing, Adv. Biochem. Eng. Biotechnol. (2007) 195–237.
[40] J. Gao, Y. Hu, S. Li, Y. Zhang, X. Chen, Tautomeric equilibrium of creatinine and creatininium cation in aqueous solutions explored by Raman spectroscopy and density functional theory calculations, Chem. Phys. (2013) 81–89.

R.K.Rakesh Kumar received his B.Sc. in Physics, Chemistry and Mathematics from Christ University, Bangalore in 2016 and is currently a Ph.D. student at Institute of Medical Science and Technology, National Sun Yat-sen University, Taiwan under the supervision of Prof. Cheng-Hsin Chuang. His current scientific interest includes designing cost effective and rapid synthesis protocols of advanced functional nanomaterials for applications in point-of-care biosensing.

Amit Kumar received his B.Sc. in Physics hons., from Delhi University, New Delhi in 2016 and is currently a Ph.D. student at Institute of Medical Science and Technology, National Sun Yat-sen University, Taiwan under the supervision of Prof. Cheng-Hsin Chuang. His current scientific interest includes nanomaterial and nanocomposite synthesis for smart point-of-care sensing applications.

Muhammad Omar Shaikh currently serves as an Assistant Professor of Sustainability Science and Engineering at Tunghai University. He completed his MEng in Materials Science and Engineering from Imperial College London in 2010 and his Ph. D. in Mechatronic Science and Engineering from the Southern Taiwan University of Science and Technology in 2015. His doctoral research involved developing earth-abundant and sustainable nanomaterials for applications like energy harvesting and targeted drug delivery. Thereafter he held two postdoctoral positions in Taiwan where he conducted highly interdisciplinary research spanning electrochemistry, micro/nano technology, smart sensing and additive manufacturing. He also previously served as the Chief Technical Officer for BiTAPE Logistics Ltd., a university spin-off company developing a printed smart tape with multiplexed sensing capability for providing IoT based logistic services.

Chen-Yi Liao is an attending physician of nephrology at Kaohsiung Armed Forces General Hospital. He graduated from National Defense Medical Center in 2009 and trained as nephrologist in Tri-service General Hospital. He specialized in the areas of nephrology including acid-base disturbance, chronic kidney disease, and diabetes nephropathy.

Cheng-Hsin Chuang is a Professor/Chair of Medical Science and Technology at National Sun Yat-sen University in Kaohsiung, Taiwan. He obtained his B.S. degree and Ph.D. degree from National Cheng Kung University (NCKU) in 1995 and 2002, respectively, both in Civil Engineering. After two-year postdoctoral fellow with Center for Micro/Nano Science and Technology at NCKU and one-year research engineer in the Smart Microsystem Technology Center at Industrial Technology Research Institute (ITRI), he was appointed to Department of Mechanical Engineering and Institute of Nanotechnology at Southern Taiwan University of Science and Technology (STUST) during 2005–2018 and promoted to Full Professor and Distinguished Professor in 2013 and 2016, respectively. Currently, He leads Micro and Nano Sensing Technology Lab (MANST Lab) and mainly dedicates in flexible electronics, AIoT for Smart Point of Care and electrochemical biosensor.